

**Chapter 2. The Strong-Field Tripodal Phosphine Donor,
[PhB(CH₂PⁱPr₂)₃], Provides Access to Electronically and Coordinatively
Unsaturated Transition Metal Complexes**

The text of this chapter is reproduced in part with permission from:

Betley, T. A.; Peters, J. C. *Inorg. Chem.* **2003**, 42, 5074.

Copyright 2003 American Chemical Society.

Abstract

This chapter introduces a sterically encumbered, strong-field tris(diisopropylphosphino)borate ligand, $[\text{PhBP}^{i\text{Pr}}_3]$ ($[\text{PhBP}^{i\text{Pr}}_3] = [\text{PhB}(\text{CH}_2\text{P}^i\text{Pr}_2)_3]$), to probe aspects of its conformational and electronic characteristics within a host of complexes. To this end, the Tl(I) complex, $[\text{PhBP}^{i\text{Pr}}_3]\text{Tl}$ (**2.1**), was synthesized and characterized in the solid-state by X-ray diffraction analysis. This precursor proves to be an effective transmetallating agent, as evidenced by its reaction with the divalent halides FeCl_2 and CoX_2 ($\text{X} = \text{Cl}, \text{I}$) to produce the monomeric, 4-coordinate, high-spin derivatives $[\text{PhBP}^{i\text{Pr}}_3]\text{FeCl}$ (**2.2**) and $[\text{PhBP}^{i\text{Pr}}_3]\text{CoX}$ ($\text{X} = \text{Cl}$ (**2.3**), I (**2.4**)) in good yield. Complexes **2.2-2.4** were each characterized by X-ray diffraction analysis and shown to be monomeric in the solid-state. For conformational and electronic comparison within a system exhibiting higher than 4-coordination, the 16-electron ruthenium complexes $\{[\text{PhBP}^{i\text{Pr}}_3]\text{Ru}(\mu\text{-Cl})\}_2$ (**2.5**) and $\{[\text{PhBP}_3]\text{Ru}(\mu\text{-Cl})\}_2$ (**2.6**) were prepared and characterized ($[\text{PhBP}_3] = [\text{PhB}(\text{CH}_2\text{PPh}_2)_3]$). The chloride complexes **2.2** and **2.8** reacted with excess CO to afford the divalent, monocarbonyl adducts $[\text{PhBP}^{i\text{Pr}}_3]\text{FeCl}(\text{CO})$ (**2.7**) and $[\text{PhBP}^{i\text{Pr}}_3]\text{CoCl}(\text{CO})$ (**2.8**), respectively. Reaction of **2.4** with excess CO resulted in the monovalent, dicarbonyl product $[\text{PhBP}^{i\text{Pr}}_3]\text{Co}^{\text{I}}(\text{CO})_2$ (**2.9**). Complexes **2.5** and **2.6** also bound CO readily, providing the octahedral, 18-electron complexes $[\text{PhBP}^{i\text{Pr}}_3]\text{RuCl}(\text{CO})_2$ (**2.10**) and $[\text{PhBP}_3]\text{RuCl}(\text{CO})_2$ (**2.11**), respectively. Dimers **2.5** and **2.6** were broken up by reaction with trimethylphosphine to produce the mono- PMe_3 adducts $[\text{PhBP}^{i\text{Pr}}_3]\text{RuCl}(\text{PMe}_3)$ (**2.12**) and $[\text{PhBP}_3]\text{RuCl}(\text{PMe}_3)$ (**2.13**). Stoichiometric oxidation of **2.3** with dioxygen provided the 4-electron oxidation product $[\text{PhB}(\text{CH}_2\text{P}(\text{O})^i\text{Pr}_2)_2(\text{CH}_2\text{P}^i\text{Pr}_2)]\text{CoCl}$ (**2.14**), while exposure of **2.3** to excess oxygen

results in the 6-electron oxidation product $[\text{PhB}(\text{CH}_2\text{P}(\text{O})^i\text{Pr}_2)_3]\text{CoCl}$ (**2.15**). Complexes **2.2** and **2.4** were characterized via cyclic voltammetry to compare their redox behavior to their $[\text{PhBP}_3]$ analogues. Complex **2.4** was also studied by SQUID magnetization and EPR spectroscopy to confirm its high-spin assignment, providing an interesting contrast to its previously described low-spin relative, $[\text{PhBP}_3]\text{CoI}$. The difference in spin states observed for these two systems reflects the conformational rigidity of the $[\text{PhBP}^{i\text{Pr}}_3]$ ligand by comparison to $[\text{PhBP}_3]$, leaving the former less able to accommodate a JT-distorted electronic ground state.

2.1. Introduction

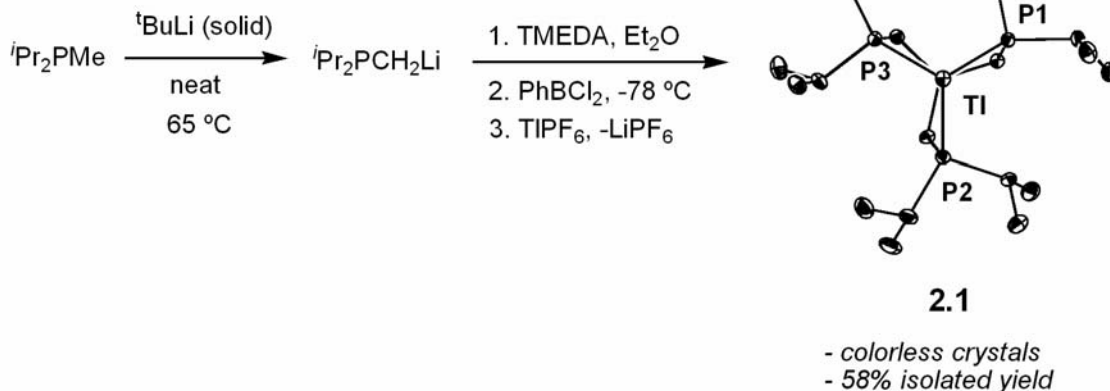
An area of ongoing interest to our group concerns the systematic preparation of pseudotetrahedral complexes that feature mid-to-late 3d ions (Mn, Fe, Co, Ni, Cu).^{1,2} While this is a very well-studied area in coordination chemistry,³ our particular interest concerns developing new, strong donor L₃ platforms that enable binding of π -acidic ligands (e.g., N₂, CO, NO⁺) and also strongly π -basic ligands (e.g., O²⁻, NR²⁻, N³⁻) in a fourth coordination site (i.e., L₃M-X where X is a π -acid or π -base). While later 3d systems that fulfill the first requirement are common,^{3e,g,4,5} those that fulfill the latter requirement are rare.² The historical incompatibility of pseudotetrahedral, later 3d ions with strongly π -basic ligands can be attributed to the high-spin ground state configurations that dominate this region of the periodic table. Complexes with strongly destabilized d-orbitals containing unpaired electrons are expected to be very reactive.

Recently, our group has shown that by using strong L₃ donor ligands with a borate unit embedded within the backbone of the ligand, 3d ions of the type L₃M \equiv E are electronically accessible (L = P, M = Fe, Co; E = NR; d-count = 5, 6).² Moreover, low-spin configurations are accessible even for d⁷ configurations in the absence of the strongly π -basic fourth donor ligand (e.g., low-spin [PhBP₃]CoI where [PhBP₃] = [PhB(CH₂PPh₂)₃]).¹ To explore related systems using more strongly donating tripodal phosphine ligands, we set out to modify the [PhBP₃] ligand scaffold by substitution of the soft aryl phosphine donors with harder, more electron-releasing alkyl phosphine donors. In this context, we now describe the preparation of the phenyl-tris(diisopropylphosphino)borate anion, [PhBP^{iPr}₃] ([PhBP^{iPr}₃] = [PhB(CH₂P^{iPr}₂)₃]), and examine aspects of its electronic and structural properties in comparison to those of the

parent [PhBP₃] ligand. Studies of this type should help us to better understand the electronic origin behind the unusual ground state configurations we have observed in these [PhBP₃] systems thus far, and will provide the impetus to exploit these new scaffolds in small molecule activation chemistry.

2.2. Results

2.2.1. Synthesis and Characterization of [PhBP^{iPr}₃][Tl] (2.1). Following effective methodology for the preparation of a host of di- and tripodal borate ligands,^{6,7,8} we sought delivery of a suitable phosphine carbanion to PhBCl₂. Our attention focused on the selective deprotonation of ⁱPr₂PMe using conditions similar to those reported by Karsch for lithiating ^tBu₂PMe.⁹ The desired lithio reagent, ⁱPr₂PCH₂Li, was obtained readily by deprotonation with solid ^tBuLi (65 °C, 12 h, 96% yield, Scheme 1). Addition of stoichiometric TMEDA (TMEDA = tetraethylmethylenediamine) to an ethereal suspension of ⁱPr₂PCH₂Li aided its partial dissolution and facilitated its subsequent delivery to PhBCl₂ to provide [PhBP^{iPr}₃][Li(TMEDA)_x]. Owing to the synthetic utility we have experienced with the thallium reagent [PhBP₃]Tl,¹ [PhBP^{iPr}₃][Li(TMEDA)_x] was directly converted to [PhBP^{iPr}₃][Tl] (**2.1**) by *in situ* addition of TlPF₆ (58% overall yield, ³¹P NMR δ 45.8 ppm, ¹J_{203 Tl-P} = 5865 Hz, ¹J_{205 Tl-P} = 5913 Hz). Complex **2.1** proved highly unstable to protic solvents including water and ethanol, and also to oxidation by oxygen. These properties contrast those of its parent complex, [PhBP₃]Tl, which can be isolated from aqueous media under an atmosphere of air without appreciable degradation.^{1b}

Scheme 2.1

Scheme 2.1. Preparation and solid-state structure of $[\text{PhBP}^{i\text{Pr}}_3]\text{Tl}$ (**2.1**) displacement ellipsoid (50%) representation of $[\text{PhBP}^{i\text{Pr}}_3]\text{Tl}$ (**2.1**) viewed down the Tl-B axis. Hydrogen atoms and borate phenyl ring have been omitted for clarity. Selected bond distances (Å) and angles (deg): Tl-P1, 2.901(1); Tl-P2, 2.921(1); Tl-P3, 2.894(1); Tl-B, 4.221(3); P1-Tl-P2, 75.25(2); P1-Tl-P3, 76.60(2); P2-Tl-P3, 77.72(2).

X-ray analysis of **2.1** confirmed a κ^3 -binding mode for the phosphine ligand to a single thallium(I) ion, similar to that of the $[\text{PhBP}_3]$ derivative. One noteworthy structural difference is that **2.1** is rigorously monomeric in the solid-state, while $[\text{PhBP}_3][\text{Tl}]$ exhibits weak Tl-Tl interactions in the solid-state.^{1b} The isopropyl substituents of **2.1** form a vertical fence around the thallium(I) center. The methyne protons are arranged such that each bisects the methyl groups of an adjacent isopropyl group. This interlocked pattern tightly gears the isopropyls in a fanlike fashion that makes complex **2.1** chiral (Scheme 2.1).

2.2.2. Synthesis of $[\text{PhBP}^{i\text{Pr}}_3]\text{M}(\text{X})$ Complexes (M = Fe, Co, Ru). Our present interest in the chemistry of **2.1** pertains to its utility in delivering the $[\text{PhBP}^{i\text{Pr}}_3]$ anion to

transition metals. The data presented here detail a number of iron, cobalt, and ruthenium complexes that collectively provide the context from which to compare steric and electronic properties between $[\text{PhBP}^{i\text{Pr}}_3]$ and $[\text{PhBP}_3]$.

Complex **2.1** underwent loss of TIX upon reaction with either FeCl_2 or CoX_2 ($\text{X} = \text{Cl}, \text{I}$) in THF solution to afford the well-defined complexes $[\text{PhBP}^{i\text{Pr}}_3]\text{FeCl}$ (**2.2**), $[\text{PhBP}^{i\text{Pr}}_3]\text{CoCl}$ (**2.3**), and $[\text{PhBP}^{i\text{Pr}}_3]\text{CoI}$ (**2.4**) (Scheme 2). Chloride **2.2** was precipitated from benzene by slow evaporation as canary-yellow crystals that were suitable for X-ray analysis (Figure 1). Crystals were similarly obtained for aqua-colored chloride **2.3** and lime-green iodide **2.4**. X-ray analysis revealed that **2.2**, **2.3**, and **2.4** are monomeric, pseudotetrahedral species in the solid-state (Figure 2.1). A detailed discussion of these crystal structures is reserved for the discussion subsections 2.3.2-3.

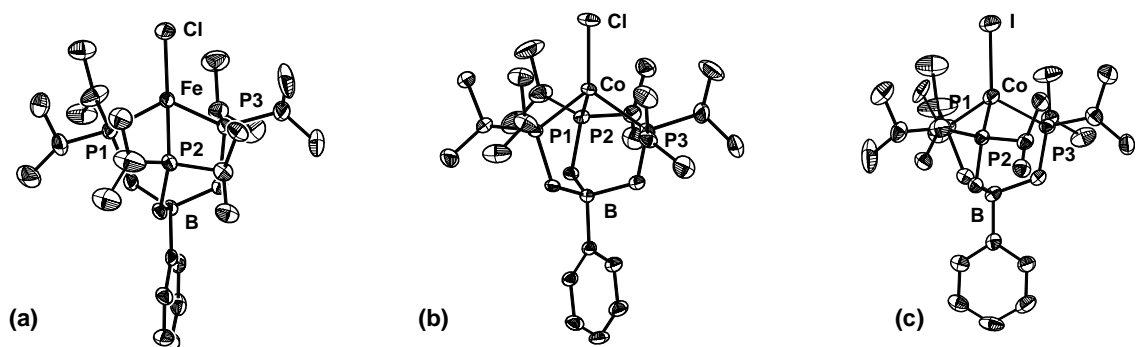


Figure 2.1. Displacement ellipsoid (50%) representation of (a) $[\text{PhBP}^{i\text{Pr}}_3]\text{FeCl}$ (**2.2**), (b) $[\text{PhBP}^{i\text{Pr}}_3]\text{CoCl}$ (**2.3**), and (c) $[\text{PhBP}^{i\text{Pr}}_3]\text{CoI}$ (**2.4**). Hydrogen atoms have been removed for clarity. Selected bond distances (Å) and angles (deg), for **2.2**: Fe-P1 2.415(1), Fe-P2 2.431(1), Fe-P3 2.428(1), Fe-Cl 2.220(1), Fe-B 3.501(3); P1-Fe-P2 93.24(3), P1-Fe-P3 94.10(3), P2-Fe-P3 94.49(3), Cl-Fe-P1 122.12(3), Cl-Fe-P2 122.62(4), Cl-Fe-P3 122.52(3). For **2.3**: Co-P1 2.334(2), Co-P2 2.332(1), Co-P3 2.330(2), Co-Cl 2.196(3), Co-B 3.363(4); P1-Co-P2 97.88(3), P1-Co-P3 96.52(3), P2-Co-P3 98.19(3), Cl-Co-P1 121.40(3), Cl-Co-P2 119.53(3), Cl-Co-P3 118.25(3). For **2.4**: Co-P1 2.334(2), Co-P2 2.321(2), Co-P3 2.385(2), Co-I 2.540(1), Co-B 3.365(3); P1-Co-P2 97.84(6), P1-Co-P3 97.55(6), P2-Co-P3 97.32(6), I-Co-P1 119.53(5), I-Co-P2 118.27(5), I-Co-P3 121.29(5).

Reaction of **2.1** with $\text{RuCl}_2(\text{PPh}_3)_3$ produced the rust-colored, 16-electron dimer $\{[\text{PhBP}^{i\text{Pr}}_3]\text{Ru}(\mu\text{-Cl})\}_2$ (**2.5**) (Scheme 2.2). Its $[\text{PhBP}_3]$ analogue, $\{[\text{PhBP}_3]\text{Ru}(\mu\text{-Cl})\}_2$ (**2.6**), was similarly prepared by reaction of $[\text{PhBP}_3]\text{Ti}$ with $\text{RuCl}_2(\text{PPh}_3)_3$. The solid-state structure of complex **2.6** was obtained (Figure 2.2) and shows two 5-coordinate $\text{Ru}(\text{II})$ centers in an approximately square-pyramidal configuration. It is interesting to note that related 16-electron dimers are not known for isosteric triphos ($\text{Me}(\text{CH}_2\text{PPh}_2)_3$) systems, nor for tris(pyrazolyl)borate analogues.^{10,11} In these latter cases, 18-electron products are more typically obtained (e.g., $\{\text{Me}(\text{CH}_2\text{PPh}_2)_3\text{Ru}\}_2(\mu\text{-Cl})_3^{2+}$, $[\text{Tp}']\text{RuCl}(\text{PR}_3)_2$).

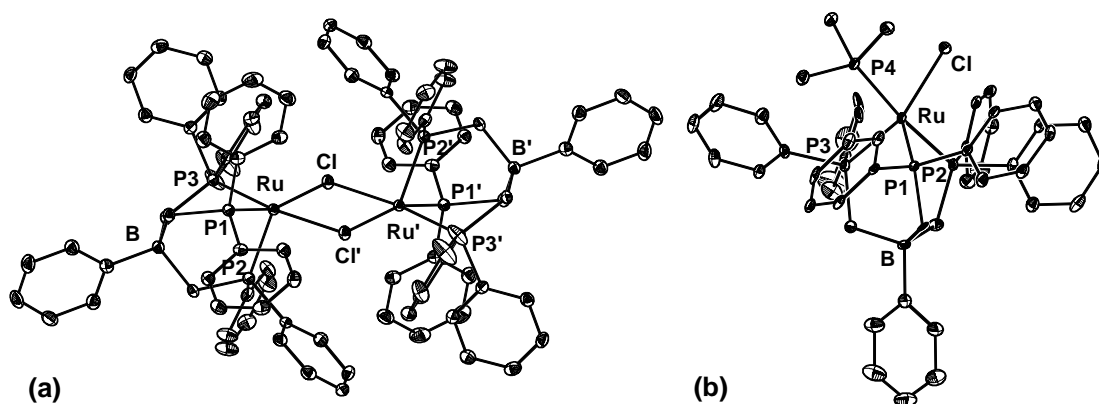
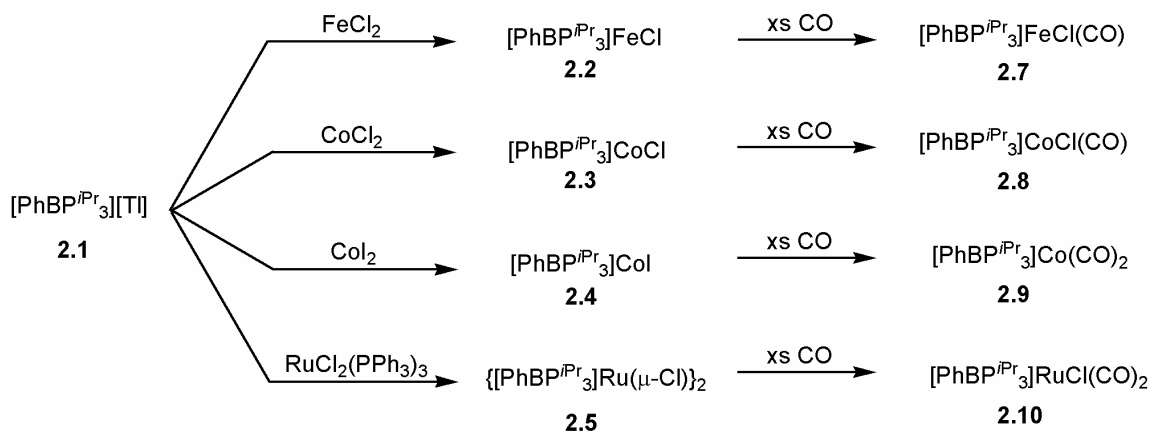


Figure 2.2. Displacement ellipsoid (50%) representation for (a) $\{[\text{PhBP}_3]\text{Ru}(\mu\text{-Cl})\}_2$ (**2.6**) and (b) $[\text{PhBP}_3]\text{RuCl}(\text{PMe}_3)$ (**2.13**). Hydrogen atoms are omitted for clarity. Selected bond distances (Å) and angles (deg), for **2.6**: Ru-Cl 2.448(1), Ru-Cl' 2.457(1), Ru-P1 2.295(1), Ru-P2 2.221(1), Ru-P3 2.271(2), P1-Ru-P2 90.40(2), P1-Ru-P3 86.37(2), P2-Ru-P3 86.92(2). For **2.13**: Ru-Cl 2.427(1), Ru-P1 2.225(1), Ru-P2 2.252(2), Ru-P3 2.400(1), Ru-P4 2.381(1), P1-Ru-P2 89.90(4), P1-Ru-P3 87.86(4), P2-Ru-P3 85.93(4).

Scheme 2.2**2.2.3. Magnetic Characterization of [PhBP^{iPr}₃]MX Complexes (M = Fe, Co).**

The complexes [PhBP₃]FeCl,^{2b} {[PhBP₃]Co(μ-Cl)}₂,^{1a} and [PhBP₃]CoI¹ have been described elsewhere. [PhBP₃]FeCl is pseudotetrahedral with an $S = 2$ ground state configuration. Likewise, [PhBP^{iPr}₃]FeCl (**2.2**) is high-spin ($5.23 \mu_B$, Evans method in benzene). The comparative magnetic data for the cobalt systems are more puzzling. In benzene solution, both [PhBP₃]CoCl and [PhBP₃]CoI are pseudotetrahedral and low-spin ($S = 1/2$). Whereas the chloride dimerizes in the solid-state, [PhBP₃]CoI remains monomeric and low-spin.^{1a} By contrast, **2.3** and **2.4** are both monomeric in the solid-state. Moreover, they are each high-spin, both in benzene solution and in the solid-state. A susceptibility determination using the Evans method provided values of 4.12 and $4.02 \mu_B$ for complexes **2.3** and **2.4**, respectively. To confirm its high-spin character at low temperature, **2.4** was also characterized by SQUID magnetometry from 5 to 300 K. As can be seen from Figure 2.3a, **2.4** maintains its quartet ground state throughout this temperature range. The Curie Law observed in this temperature range (indicated by χ_m^{-1} vs T , Figure 2.3b) indicates that the $3/2$ spin state is the only state that is thermally populated.

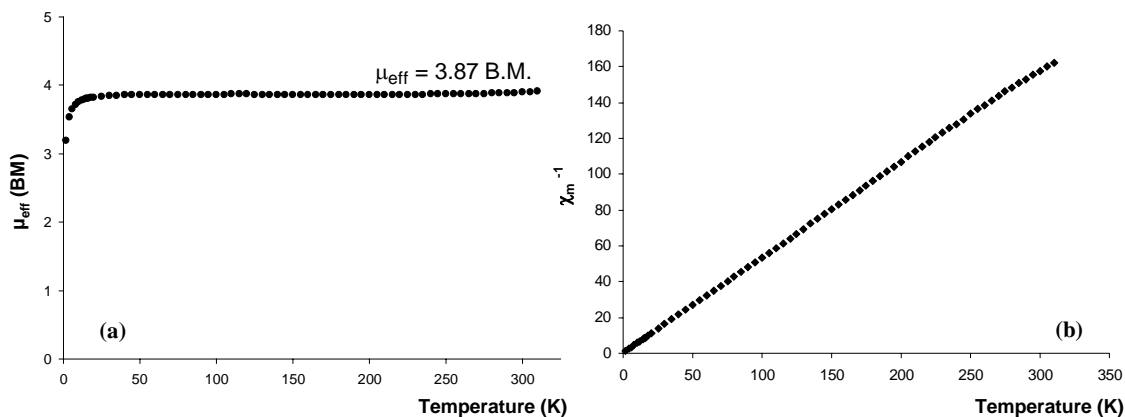


Figure 2.3. (a) SQUID magnetization data shown as a plot of μ_{eff} (BM) versus T (K), and (b) as a plot of χ_m^{-1} (mol/cm^3) versus T (K), for $[\text{PhBP}^{i\text{Pr}}_3]\text{CoI}$ (**2.4**).

The glassy toluene EPR spectrum of **2.4** was also collected at 4 K, shown in Figure 2.4 for comparison with the spectrum previously reported for $[\text{PhBP}_3]\text{CoI}$.^{1a} The spectrum for **2.4** shows a strong, signature signal in the region $g \sim 4.8$ ($H = 120 \text{ mT}$), characteristic of a high-spin Co(II) system.¹² Another signal is present in the region $g \sim 2.2$ ($H = 320 \text{ mT}$) that features apparent hyperfine coupling due to the Co ($S = 7/2$), and possibly the P ($S = 1/2$) nuclei.^{13,14} As expected for an $S = 3/2$ Co(II) system,^{1a,15} no signal was observed at ambient temperature. By contrast, the glassy toluene EPR spectrum of doublet $[\text{PhBP}_3]\text{CoI}$ did not feature a signal in the region $g \sim 4.8$ and afforded an isotropic signal in the region $g \sim 2.0$ even at $22 \text{ }^\circ\text{C}$.^{1a} The characteristic high-spin signal at $g \sim 4.8$ appeared only when $[\text{PhBP}_3]\text{CoI}$ was oxidized to $[\text{PhB}(\text{CH}_2\text{PPh}_2)(\text{CH}_2\text{P}(\text{O})\text{Ph}_2)_2]\text{CoI}$, a rigorously high-spin product.^{1a}

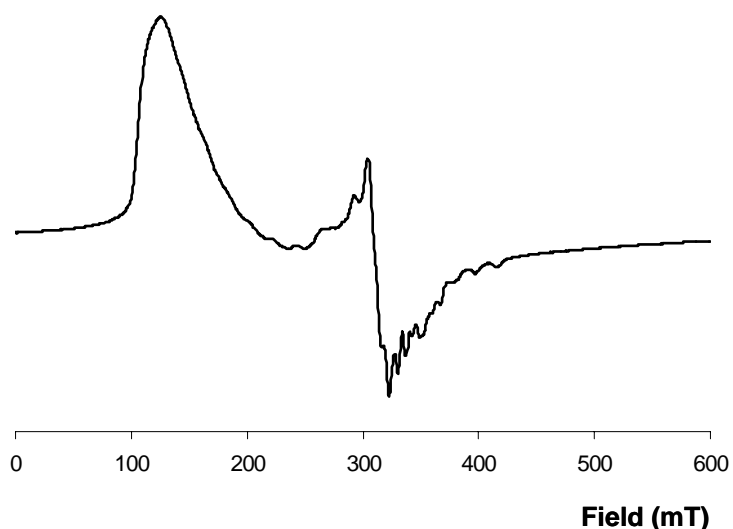


Figure 2.4. EPR spectrum of **2.4** in glassy toluene (4 K, X-band, 9.62 GHz).

2.2.4. Electrochemical Comparisons between $[\text{PhBP}^{i\text{Pr}}_3]\text{MX}$ and $[\text{PhBP}_3]\text{MX}$

(**M** = **Fe**, **Co**). To assess the relative electron-releasing character of the $[\text{PhBP}^{i\text{Pr}}_3]$ and $[\text{PhBP}_3]$ anions, we examined the cyclic voltammetry of the respective Fe(II) chloride and Co(II) iodide complexes. The cyclic voltammograms for $[\text{PhBP}^{i\text{Pr}}_3]\text{FeCl}$ and $[\text{PhBP}_3]\text{FeCl}$ are presented in Figure 2.5, labeled a and b, respectively. The parent complex, $[\text{PhBP}_3]\text{FeCl}$, shows a fully reversible $\text{Fe}^{\text{II/I}}$ couple at -1.68 V vs. Fc/Fc^+ (Figure 2.5). The $\text{Fe}^{\text{II/I}}$ couple at -2.03 V for $[\text{PhBP}^{i\text{Pr}}_3]\text{FeCl}$ (Figure 2.5a) appears to be only quasireversible (50 mV/s), suggesting that some degradation or reaction of the anion $[\{\text{PhBP}^{i\text{Pr}}_3\}\text{FeCl}]^-$ occurs on this time scale. The striking 322 mV shift observed for the $\text{Fe}^{\text{II/I}}$ couple of **2.2** by comparison to that of $[\text{PhBP}_3]\text{FeCl}$ speaks to the marked increase in electron-releasing character that occurs when six isopropyl groups replace six phenyl groups at the phosphine donor positions.

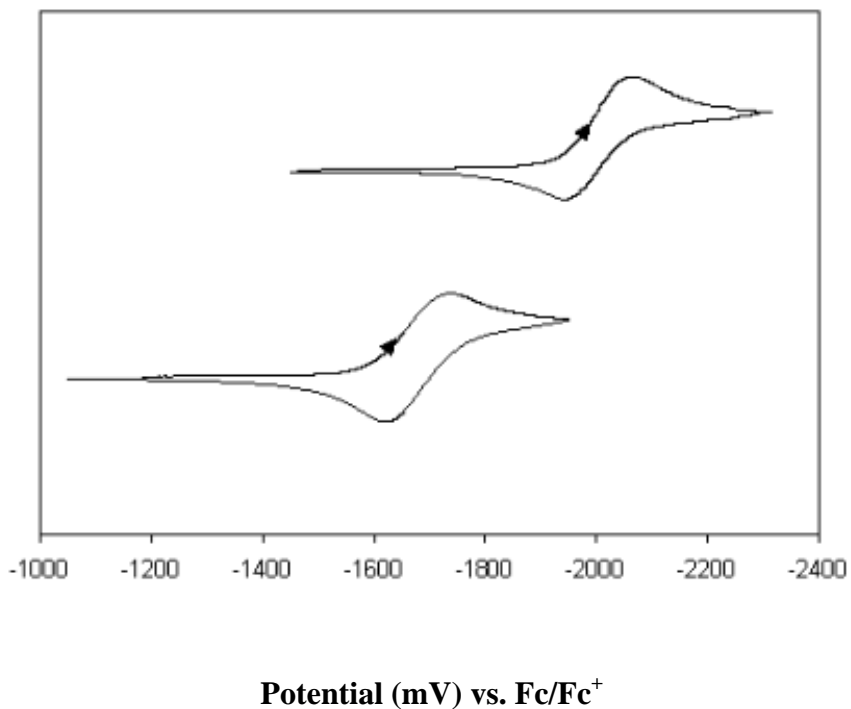


Figure 2.5. Cyclic voltammetry of (top) $[\text{PhBP}^{i\text{Pr}}_3]\text{FeCl}$ (**2.2**) and (bottom) $[\text{PhBP}_3]\text{FeCl}$ in 0.4 M $[\text{TBA}][\text{PF}_6]/\text{THF}$, scan rate = 50 mV/s, V vs. Fc/Fc^+ .

The comparative voltammograms for the compounds $[\text{PhBP}^{i\text{Pr}}_3]\text{CoI}$ and $[\text{PhBP}_3]\text{CoI}$ follow a similar trend. The more electron-releasing nature of the $[\text{PhBP}^{i\text{Pr}}_3]$ anion by comparison to the $[\text{PhBP}_3]$ anion makes it more difficult to reduce $[\text{PhBP}^{i\text{Pr}}_3]\text{CoI}$ (**2.4**) than $[\text{PhBP}_3]\text{CoI}$ by one electron. A reversible $\text{Co}^{\text{III/I}}$ couple was observed for $[\text{PhBP}_3]\text{CoI}$ at -0.97 mV, and a reversible $\text{Co}^{\text{III/I}}$ couple for **2.4** was observed at -1.32 V (Figure 2.6). Oxidation waves for each complex were also observed. A quasireversible wave (50 mV/s) is observed at -0.11 V for iodide **2.4**, whereas a fully reversible wave is observed at lower potential (-42 mV) for $[\text{PhBP}_3]\text{CoI}$. We assign each of these waves to a $\text{Co}^{\text{III/I}}$ redox process.

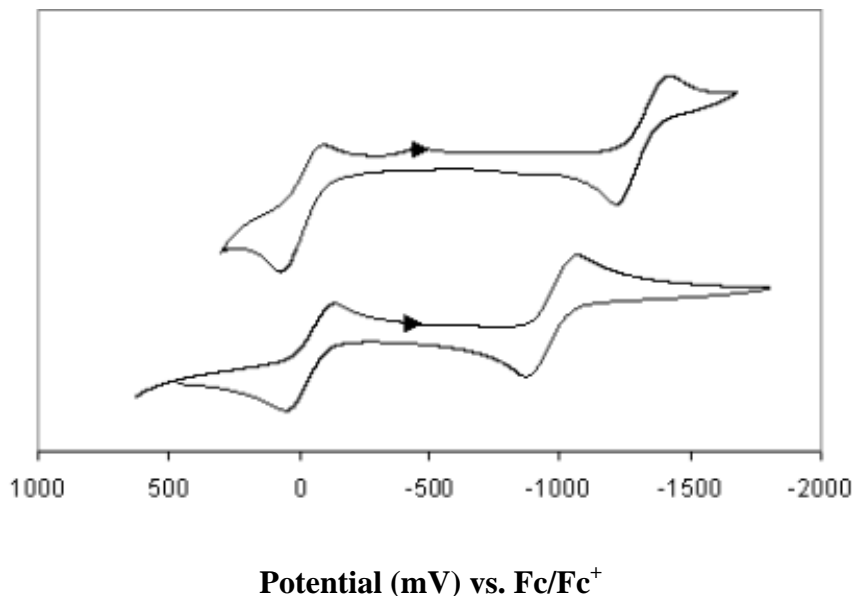


Figure 2.6. Cyclic voltammetry of (top) $[\text{PhBP}^{i\text{Pr}}_3]\text{CoI}$ (**2.4**) and (bottom) $[\text{PhBP}_3]\text{CoI}$ in 0.4 M $[\text{TBA}][\text{PF}_6]/\text{THF}$, scan rate = 50 mV/s, V vs. Fc/Fc^+ .

2.2.5. Reactivity toward CO, O₂, and PMe₃. Exposure of the iron chloride **2.2** to excess carbon monoxide resulted in the rapid formation of a 5-coordinate, diamagnetic monocarbonyl adduct, $[\text{PhBP}^{i\text{Pr}}_3]\text{FeCl}(\text{CO})$ (**2.7**) (Scheme 2.2). The 5-coordinate nature of **2.7** is noteworthy given that exposure of its $[\text{PhBP}_3]$ congener produces the octahedral, dicarbonyl adduct $[\text{PhBP}_3]\text{FeCl}(\text{CO})_2$.¹⁶ The cobalt chloride **2.3** reacted in a similar fashion upon exposure to excess carbon monoxide to produce $[\text{PhBP}^{i\text{Pr}}_3]\text{CoCl}(\text{CO})$ (**2.8**) ($\mu_{\text{eff}} = 2.24 \mu_{\text{B}}$) (Scheme 2.2). While the structures of **2.7** and **2.8** were not determined, we presume each to be approximately trigonal bipyramidal, with the chloride ligand coordinated in an equatorial position and the CO bound axially, as is found for the structurally characterized complex $[\text{PhBP}_3]\text{CoBr}(\text{CO})$.¹⁷ Iodide **2.4** underwent rapid reduction on CO exposure to generate the monovalent dicarbonyl complex $[\text{PhBP}^{i\text{Pr}}_3]\text{Co}(\text{CO})_2$ (**2.9**).

The ruthenium dimers **2.5** and **2.6** were broken up on exposure to carbon monoxide to form the octahedral, dicarbonyl adducts $[\text{PhBP}^{i\text{Pr}}_3]\text{RuCl}(\text{CO})_2$ (**2.10**) and $[\text{PhBP}_3]\text{RuCl}(\text{CO})_2$ (**2.11**), respectively. Both **2.5** and **2.6** were also broken up when heated in the presence of trimethylphosphine to provide the monophosphine adducts $[\text{PhBP}^{i\text{Pr}}_3]\text{RuCl}(\text{PMe}_3)$ (**2.12**) and $[\text{PhBP}_3]\text{RuCl}(\text{PMe}_3)$ (**2.13**), respectively. The latter complex, **2.13**, was examined crystallographically and shown to be approximately trigonal-bipyramidal. Its chloride ligand occupies an axial position, and the PMe_3 ligand occupies an equatorial site (Figure 2.2). It is again underscored that analogous 5-coordinate, 16-electron complexes of ruthenium supported by tris(pyrazolyl)borate ligands are not known, even for cases where sterically encumbering derivatives of the ligand have been employed.¹¹

Exposure of **2.3** in solution or in the solid-state to stoichiometric dioxygen led to the rapid, 4-electron oxidation of **2.3** to produce $[\text{PhB}(\text{CH}_2\text{P}(\text{O})^i\text{Pr}_2)_2(\text{CH}_2\text{P}^i\text{Pr})]\text{CoCl}$ (**2.14**). Reaction of **2.3** with excess dioxygen produced a 6-electron oxidation product, the tris(phosphineoxide) complex $[\text{PhB}(\text{CH}_2\text{P}(\text{O})^i\text{Pr}_2)_3]\text{CoCl}$ (**2.15**). The 4-electron oxidation product **2.14** is reminiscent of the only observed oxidation products when $[\text{PhBP}_3]\text{CoX}$ complexes are exposed to excess oxygen. The 6-electron oxidation product **2.15** is unique to the $[\text{PhBP}^{i\text{Pr}}_3]$ system.^{1a,18} Both complexes **2.14** and **2.15** have been characterized by X-ray analysis, and their solid-state structures are shown in Figure 2.7. While we have yet to pursue the chemistry of $[\text{PhB}(\text{CH}_2\text{P}(\text{O})\text{R}_2)_3]^-$ ligands systematically, it should be possible to realize their preparation, and that of their sulfur analogues $[\text{PhB}(\text{CH}_2\text{P}(\text{S})\text{R}_2)_3]^-$, independently.^{7c} The solid-state structure of **2.15** suggests that these latter ligand classes may well be worthy of pursuit.

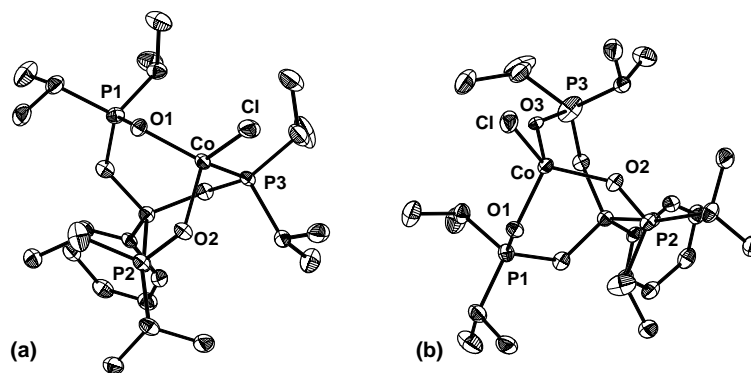


Figure 2.7. Displacement ellipsoid (50%) representation of (a) $[\text{PhB}(\text{CH}_2\text{P}(\text{O})^i\text{Pr}_2)_2(\text{CH}_2\text{P}^i\text{Pr})]\text{CoCl}$ (**2.14**) and (b) $[\text{PhB}(\text{CH}_2\text{P}(\text{O})^i\text{Pr}_2)_3]\text{CoCl}$ (**2.15**). The hydrogen atoms of each complex have been omitted for clarity. Selected bond distances (Å), for **2.14**: Co-Cl 2.223(1), Co-O1 1.955(2), Co-O2 1.965(1), Co-P3 2.410(4). For **2.15**: Co-Cl 2.223(1), Co-O1 1.955(2), Co-O2 1.965(1), Co-O3 1.739(2).

2.3. Discussion

2.3.1. Relative Electron-Releasing Character of $[\text{PhBP}^{i\text{Pr}}_3]$. The formation of the carbonyl species **2.7-2.11** provides an additional platform by which to compare the relative reducing nature of the $[\text{PhBP}^{i\text{Pr}}_3]$ and $[\text{PhBP}_3]$ anions. The difference in CO stretching frequencies of 26 cm^{-1} between $[\text{PhBP}_3]\text{Co}(\text{CO})(\text{Cl})$ ¹⁷ and **2.8** (see entries 3 and 2 in Table 2.1, respectively) underscores the stronger electron-releasing character of the $[\text{PhBP}^{i\text{Pr}}_3]$ anion by comparison to its $[\text{PhBP}_3]$ relative. A similar trend is observed between dicarbonyl **2.9** and previously reported $[\text{PhBP}_3]\text{Co}(\text{CO})_2$ (see entries 4 and 5). These latter two complexes provide for an interesting comparison to other facially capping ligands. The infrared data for the related complexes $[\text{Tp}^{3-i\text{Pr}-5\text{Me}}]\text{Co}(\text{CO})_2$,¹⁹ $\text{CpCo}(\text{CO})_2$,²⁰ and $\text{Cp}^*\text{Co}(\text{CO})_2$ ²¹ are also recorded in Table 1 ($[\text{Tp}^{3-i\text{Pr}-5\text{Me}}]$ = hydrotris(3-isopropyl-5-methylpyrazolyl)borate). Most noteworthy is that dicarbonyl **2.9** exhibits the

lowest carbonyl stretching frequencies of the series, surpassing even that of the Cp* derivative. It is apparent that [PhBP^{*i*Pr}₃] is a highly electron-releasing ligand.

We examined the octahedral carbonyl complexes provided by the Ru(II) scaffold (entries 10-15, Table 2.1). Like the cobalt series, there is a strong reduction in the carbonyl stretching frequency on moving from [PhBP₃]RuCl(CO)₂ (**2.11**) to [PhBP^{*i*Pr}₃]RuCl(CO)₂ (**2.10**) (entries 13 and 11 in Table 2.1, respectively). The more noteworthy distinction in this series is that the Cp* system features CO vibrations that are in fact lowest in energy, emphasizing the need to define a specific geometric model system when trying to correlate infrared data to the relative electron-releasing character of a set of ligands. Infrared data for the cationic triphos complexes [(triphos)Co(CO)₂][PF₆]²² and [(triphos)RuCl(CO)₂][PF₆]²³ are presented to highlight the large difference in ν_{CO} between these cations and their neutral congeners, [PhBP₃]Co(CO)₂ and [PhBP₃]RuCl(CO)₂ (triphos = CH₃C(CH₂PPh₂)₃). Related infrared model data for bidentate (amino)- and (phosphine)borate systems have been catalogued elsewhere.²⁴

Table 2.1. Carbonyl stretching frequencies for (κ^3 -L)Co(CO)₂ and (κ^3 -L)RuCl(CO)₂.

Entry	Complex	ν_{CO} (cm ⁻¹)	Ref.
1	[PhBP ^{iPr} ₃]FeCl(CO)	2020 ^a	--
2	[PhBP ^{iPr} ₃]CoCl(CO)	2010 ^a	--
3	[PhBP ₃]CoCl(CO)	2036 ^a	--
4	[PhBP ^{iPr} ₃]Co(CO) ₂	1990, 1904 ^a	--
5	[PhBP ₃]Co(CO) ₂	2008, 1932 ^a	2
6	(Cp*)Co(CO) ₂	2011, 1949 ^b	21
7	[Tp ^{3-iPr-5Me}]Co(CO) ₂	2016, 1939 ^c	19
8	(Cp)Co(CO) ₂	2033, 1972 ^b	20
9	[(triphos)Co(CO) ₂][PF ₆]	2030, 1972 ^d	22
10	(Cp*)RuCl(CO) ₂	2028, 1974 ^e	25
11	[PhBP ^{iPr} ₃]RuCl(CO) ₂	2045, 1993 ^a	--
12	(Cp)RuCl(CO) ₂	2059, 2008 ^d	26
13	[PhBP ₃]RuCl(CO) ₂	2068, 2021 ^d	--
14	[Tp]RuCl(CO) ₂	2071, 2011 ^d	27
15	[(triphos)RuCl(CO) ₂][PF ₆]	2076, 2043 ^d	23

^a Benzene/KBr; ^b Cyclohexane/KBr; ^c Toluene/KBr; ^d CH₂Cl₂/KBr; ^e THF/KBr

2.3.2. Conformational Considerations. Of obvious concern is to consider the relative steric influences exerted by the [PhBP₃] and the [PhBP^{iPr}₃] anions. [PhBP^{iPr}₃]FeCl (**2.2**) and [PhBP₃]FeCl afford an excellent and unambiguous opportunity to consider steric and conformational characteristics of the [PhBP₃] and [PhBP^{iPr}₃]

ligands, as they feature the same divalent first row ion in a common electronic configuration. Inspection of the structure of $[\text{PhBP}^{i\text{Pr}}_3]\text{FeCl}$ (**2.2**) reveals that its Fe-P bond distances are remarkably similar to those of the reported $[\text{PhBP}_3]\text{FeCl}$ complex^{2b} (complex **2.2**, Fe-P1 2.415(1), Fe-P2 2.431(1), Fe-P3 2.428(1) Å; $[\text{PhBP}_3]\text{FeCl}$, Fe-P1 2.419(1), Fe-P2 2.435(1), Fe-P3 2.426(1) Å). Comparison of the P-Fe-P and the Cl-Fe-P bond angles between the two iron complexes, however, establishes **2.2** to be appreciably more symmetric in nature than its $[\text{PhBP}_3]$ analogue. This detail is most obvious by inspection of the respective Cl-Fe-P bond angles. Whereas for **2.2** the three Cl-Fe-P bond angles are effectively equivalent (122.12(3)°, 122.62(4)°, and 122.52(3)°), for $[\text{PhBP}_3]\text{FeCl}$ one of these angles (110.60(3)°) is ca. 20° smaller than the other two (129.55(4)° and 129.69(4)°). It is perhaps most instructive to consider space-filling models of each of the iron complexes. Space-filling representations with views down the respective Cl-Fe-B axes are shown in Figure 2.8. The aryl groups in $[\text{PhBP}_3]\text{FeCl}$ are splayed in various directions about the Fe-P core. Two of the phenyl substituents are appreciably skewed from the molecule's vertical axis, while the larger isopropyl units of **2.2** maintain a rigid, parallel orientation to the Fe-Cl axis. The isopropyl groups of **2.2** are far more tightly packed and closely interlocked to apparently minimize energetically unfavorable steric interactions. The two space-filling models persuasively suggest that the $[\text{PhBP}^{i\text{Pr}}_3]$ ligand is conformationally much more rigid than its $[\text{PhBP}_3]$ analogue. While this conclusion should perhaps be regarded as intuitively obvious, its emphasis is important with respect to the explanation we provide for the distinctly different spin states observed for the divalent cobalt halides of each ligand type.

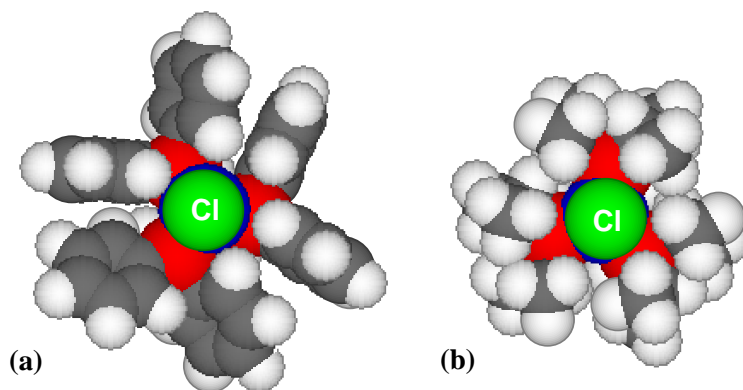


Figure 2.8. Space-filling models of (a) $[\text{PhBP}_3]\text{FeCl}$ and (b) $[\text{PhBP}^{i\text{Pr}}_3]\text{FeCl}$ (**2.2**) generated from X-ray crystal structures.

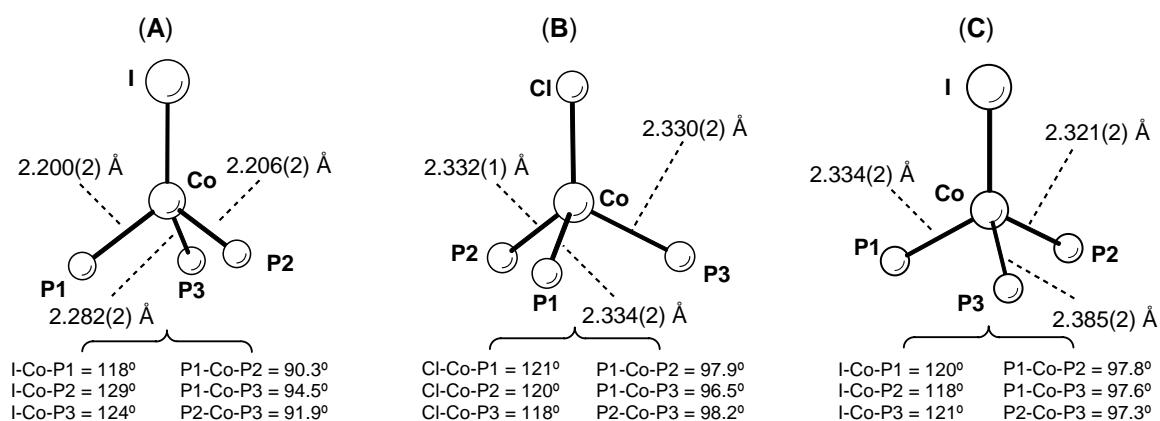


Figure 2.9. Structural representations of the immediate coordination sphere of (A) $[\text{PhBP}_3]\text{CoI}$, (B) $[\text{PhBP}^{i\text{Pr}}_3]\text{CoCl}$ (**2.3**), and (C) $[\text{PhBP}^{i\text{Pr}}_3]\text{CoI}$ (**2.4**) to aid the discussion presented in section 2.3.2-3.

2.3.3. Consideration of the Different Spin States Observed for $[\text{PhBP}_3]\text{CoI}$ and $[\text{PhBP}^{i\text{Pr}}_3]\text{CoI}$. We have previously suggested that the unusual low-spin configuration of $[\text{PhBP}_3]\text{CoI}$ arises from its strong donor strength, coupled with a pronounced axial distortion along the Co-I bond vector away from tetrahedral bond angles.^{1a} The axial distortion in $[\text{PhBP}_3]\text{CoI}$ affords average P-Co-P angles that approach

90°. These angles serve to minimize antibonding overlap between the σ -donor orbitals of the phosphines, and the central torus lobe of a d_z^2 type orbital at the cobalt center (note: the z -axis is placed along the Co-I vector; see Figure 2.10). These factors are consequences of the ligand-field and geometric constraints dictated by the [PhBP₃] ligand. The donor strength provided by [PhBP^{*i*Pr}₃] should be even stronger than for [PhBP₃], as suggested from the carbonyl model complexes discussed above, and from the electrochemical data described for the iron complexes [PhBP^{*i*Pr}₃]FeCl (**2.2**) and [PhBP₃]FeCl. It was to be expected that the monomeric [PhBP^{*i*Pr}₃]CoX halides **2.3** and **2.4** would exhibit low-spin configurations by analogy to their monomeric [PhBP₃]CoX cousins. This turns out not to be the case. The [PhBP^{*i*Pr}₃]CoX complexes are rigorously high-spin, presenting somewhat of a paradox that we think can be explained by considering the ability of the two tripodal ligand sets to geometrically accommodate a Jahn-Teller distortion. To aid consideration of the following arguments, the core atoms of the previously reported structure of [PhBP₃]CoI are shown alongside those of **2.3** and **2.4** in Figure 2.9.

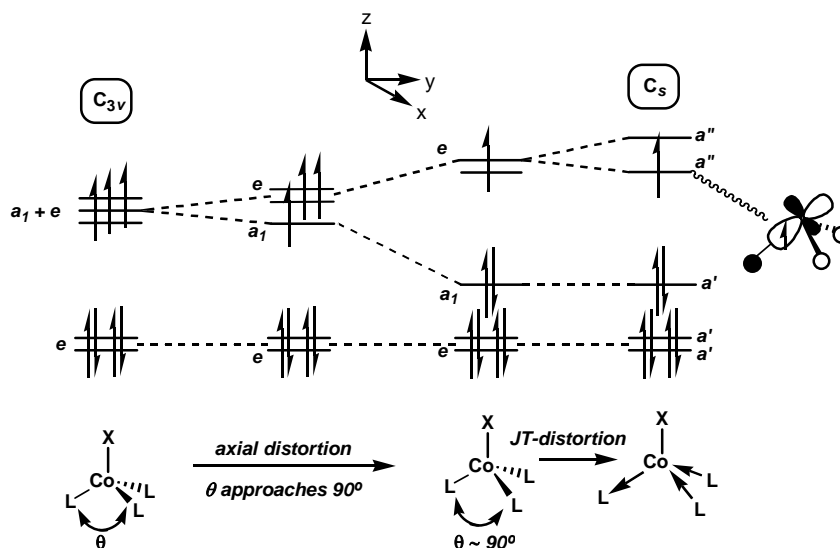


Figure 2.10. Qualitative orbital correlation diagram that illustrates the origin and nature of the JT-distortion observed in the solid-state structure of $[\text{PhBP}_3]\text{CoI}$, but not in the structures of $[\text{PhBP}^{i\text{Pr}}_3]\text{CoCl}$ (**2.3**) and $[\text{PhBP}^{i\text{Pr}}_3]\text{CoI}$ (**2.4**).

The high, nearly ideal 3-fold symmetry of $[\text{PhBP}^{i\text{Pr}}_3]\text{CoCl}$ (**2.3**) is consistent with its high-spin electronic configuration. The structure reveals three virtually equivalent Co-P bond lengths (Co-P1 2.334(2), Co-P2 2.332(1), Co-P3 2.330(2) Å). Its three X-Co-P bond lengths (average Cl-Co-P = 119.7°) and its three P-Co-P angles (average = 97.5°) also display very little variance. The same may in general be said of high-spin $[\text{PhBP}^{i\text{Pr}}_3]\text{CoI}$ (**2.4**). While in the latter complex there is a slightly more notable spread in the Co-P bond distances (Co-P1 2.334(2), Co-P2 2.321(2), Co-P3 2.385(2) Å), once again the variance in its three X-Co-P and P-Co-P bond angles is trivial, and the average of each is analogous to that for the chloride (average I-Co-P = 119.7°; P-Co-P = 97.6°). The variance in these angles and in the Co-P bond lengths observed for the parent iodide, $[\text{PhBP}_3]\text{CoI}$, is much more striking. The average of its P-Co-P angles (92.2°) is on average 5° smaller than for the high-spin systems, and a large variation in the I-Co-P bond angles (118°, 129°, and 124°) is also observed. The smaller average P-Co-P angle

observed in $[\text{PhBP}_3]\text{CoI}$ likely reflects its ability to accommodate the low-spin configuration. The closer these angles are to 90° , the smaller the overlap of the phosphine donor ligands with the central torus of the $3d_z^2$ type orbital. The doublet ground state of $[\text{PhBP}_3]\text{CoI}$ also requires that it accommodate a Jahn-Teller distortion. This is reflected in its asymmetric solid-state structure. Two short (P1 and P2) and one elongated (P3) Co-P bonds manifest a gentle distortion akin to an e-vibrational mode under 3-fold symmetry that serves to stabilize a cobalt-based orbital that is antibonding with respect to a phosphine donor and that houses a single unpaired electron. A lobal representation of this orbital is shown to the right in Figure 2.10. The three I-Co-P angles of $[\text{PhBP}_3]\text{CoI}$ also highlight its overall asymmetry. If we assume that the doublet state of $[\text{PhBP}_3]\text{CoI}$ is not too far in energy from its higher lying quartet state, accommodating a JT-distortion would seem to require that the $[\text{PhBP}_3]$ ligand be able to adjust its conformation with little energetic cost. As is suggested from the conformational description of the iron chloride complexes, different conformations of the $[\text{PhBP}_3]$ ligand would seem energetically easy to accommodate.

Inspection of the structure of **2.4** reveals it to be distinctly more symmetric in nature. Foremost, the Co-I bond is noticeably lengthened in **4** (2.540(1) Å) from that observed for $[\text{PhBP}_3]\text{CoI}$ (2.474 Å) due to its expanded high-spin radius. The I-Co-P bond angles of **2.4** are virtually indistinguishable from **2.3** and, ignoring the PhB-backbone, nearly an ideal 3-fold axis runs through the Co-I bond vector of **2.4**, evidenced by its nearly identical P-Co-P bond angles.

We suggest that the ability of the $[\text{PhBP}_3]$ ligand to conformationally accommodate a JT-distorted doublet state — a distortion that would likely be

energetically more expensive for the bulkier $[\text{PhBP}^{i\text{Pr}}_3]$ system — is the key difference that gives rise to their different spin states. Other differences might also contribute, such as a decreased π -acidity in the $[\text{PhBP}^{i\text{Pr}}_3]$ ligand versus the $[\text{PhBP}_3]$ ligand, but a steric explanation seems most plausible. In the absence of steric consequences, we would have expected the high-lying pair of orbitals that are π^* in character with respect to the phosphine donors to be more strongly destabilized in the $[\text{PhBP}^{i\text{Pr}}_3]\text{CoX}$ system, which would render it even more likely to accommodate a low-spin ground state. The difference in energy between the high- and low-spin ground states in these pseudotetrahedral d^7 systems is presumably small (i.e., between ca. 100 and 1000 cm^{-1}). This is a reasonable supposition, especially given that the low-spin $[\text{PhBP}_3]\text{CoX}$ complexes are unique with respect to their doublet configurations, and that structurally related high-spin systems are also accessible. Theopold and Doren have provided support to these assertions by theoretically examining a $[\text{Tp}]\text{CoI}$ model system that, while having an experimentally observed high-spin state, is theoretically predicted to have a low-spin state that is very close in energy.⁴ The consequence of these collective assertions is that it should be possible to prepare pseudotetrahedral cobalt(II) species that exhibit spin-crossover. Efforts to elucidate such a species are now under way.

2.4. Experimental Section

2.4.1. General Considerations. All manipulations were carried out using standard Schlenk or glovebox techniques under a dinitrogen atmosphere. Unless otherwise noted, solvents were deoxygenated and dried by thorough sparging with N_2 gas followed by passage through an activated alumina column. Nonhalogenated solvents were typically tested with a standard purple solution of sodium benzophenone ketyl in

tetrahydrofuran in order to confirm effective oxygen and moisture removal. The reagents TlPF₆, CoI₂, CoCl₂, FeCl₂, and ⁱPr₂PCl were purchased from commercial vendors and used without further purification (metal reagents from Strem Chemicals; phosphine from Aldrich). The Ru^{II} precursor RuCl₂(PPh₃)₃ was synthesized as described previously.²⁸ PhBCl₂ was purchased from Aldrich and distilled under N₂ prior to use. [PhBP₃]Tl was prepared as previously described.^{1b} Deuterated solvents were degassed and stored over activated 3-Å molecular sieves prior to use. Elemental analyses were carried out at Desert Analytics, Tucson, Arizona. NMR spectra were recorded at ambient temperature on Varian Mercury 300 MHz, Joel 400 MHz, and Inova 500 MHz spectrometers, unless otherwise noted. ¹H and ¹³C NMR chemical shifts were referenced to residual solvent. ³¹P NMR, ¹¹B NMR, and ¹⁹F NMR chemical shifts are reported relative to an external standard of 85% H₃PO₄, neat BF₃·Et₂O, and neat CFCl₃, respectively. IR spectra were recorded on a Bio-Rad Excalibur FTS 3000 spectrometer controlled by Win-IR Pro software. MS data for samples were obtained by injection of a hydrocarbon solution into a Hewlett-Packard 1100MSD mass spectrometer (ES⁺) or an Agilent 5973 mass selective detector (EI). UV-vis measurements were taken on a Hewlett-Packard 8452A diode array spectrometer using a quartz crystal cell with a Teflon cap. X-ray diffraction studies were carried out in the Beckman Institute Crystallographic Facility on a Bruker Smart 1000 CCD diffractometer.

2.4.2. Magnetic Measurements. Measurements were recorded using a Quantum Designs SQUID magnetometer running MPMSR2 software (Magnetic Property Measurement System Revision 2). Data were recorded at 5000 G. Samples were suspended in the magnetometer in plastic straws sealed under nitrogen with Lilly No. 4

gel caps. Loaded samples were centered within the magnetometer using the DC centering scan at 35 K and 5000 gauss. Data were acquired at 2-10 K (one data point/2 K), 10-60 K (one data point/5 K), 60-310 K (one data point/10 K).

$$\chi_m = \frac{\chi M}{mG} \quad \text{Eqn 2.1}$$

$$\mu_{\text{eff}} = \sqrt{7.997 \chi_m T} \quad \text{Eqn 2.2}$$

The magnetic susceptibility was adjusted for diamagnetic contributions using the constitutive corrections of Pascal's constants and a fixed temperature independent paramagnetism (TIP) crudely set to $2 \times 10^{-4} \text{ cm}^3 \text{ mol}^{-1}$.²⁹ The molar magnetic susceptibility (χ_m) was calculated by converting the calculated magnetic susceptibility (χ) (or magnetization) obtained from the magnetometer to a molar susceptibility using the multiplication factor [molecular weight (M)]/[sample weight (m) \times field strength (G)]. Curie-Weiss behavior was verified by a plot of χ_m^{-1} versus T (Figure 2.3b). Data were analyzed using equations 2.1 and 2.2. Average magnetic moments were taken from the average of magnetic moments from the ranges indicated in the Experimental Section for each complex. The Weiss constant (χ) was taken as the x -intercept of the plot of χ_m^{-1} versus T . Error bars were established at 95% confidence using regression analysis or taking two standard deviations from the mean. Solution magnetic moments were measured by the Evans method and were adjusted for diamagnetic contributions using the constitutive corrections of Pascal's constants. Averaged g -factors can be extracted from the susceptibility data, assuming zero orbital contributions, using the following equation (Eqn 2.3):

$$\chi_m = \frac{Ng^2\beta^2}{3kT}(S(S+1)) \quad \text{Eqn 2.3}$$

2.4.3. EPR Measurements. X-band EPR spectra were obtained on a Bruker EMX spectrometer equipped with a rectangular cavity working in the TE₁₀₂ mode. Variable temperature measurements were conducted with an Oxford continuous-flow helium cryostat (temperature range 3.6-300 K). Accurate frequency values were provided by a frequency counter built in the microwave bridge. Solution spectra were acquired in toluene for all of the complexes. Sample preparation was performed under a nitrogen atmosphere.

2.4.4. X-ray Crystallography Procedures. X-ray quality crystals were grown as indicated in the experimental procedures per individual complex. The crystals were mounted on a glass fiber with Paratone N oil. Structures were determined using direct methods with standard Fourier techniques using the Bruker AXS software package. In some cases, Patterson maps were used in place of the direct methods procedure. Table 2.2 includes the X-ray diffraction experimental details.

Table 2.2. X-ray diffraction experimental details for [PhBP^{iPr}₃][Ti] (**2.1**), [PhBP^{iPr}₃]FeCl (**2.2**), [PhBP^{iPr}₃]CoCl (**2.3**), [PhBP^{iPr}₃]CoI (**2.4**), {[PhBP₃]Ru(μ-Cl)}₂ (**2.6**), [PhBP₃]RuCl(PMe₃) (**2.13**), and crystal sample for **2.14** and **2.15**.

	2.1	2.2 ·C ₆ H ₆	2.3	2.4	2.6 ·2 THF	2.13	2.14 & 2.15
Chemical Formula	C ₂₇ H ₅₃ BP ₃ Tl	C ₃₃ H ₅₉ BClFeP ₃	C ₂₇ H ₅₃ BClCoP ₃	C ₂₇ H ₅₃ BCoIP ₃	C ₉₈ H ₉₈ B ₂ Cl ₂ O ₂ P ₆ Ru ₂	C ₄₈ H ₅₀ BCIP ₄ Ru	C ₂₇ H ₅₃ BClCoO ₂ P ₃
Formula Weight	685.78	650.82	575.79	667.28	1788.24	898.14	610.51
T (°C)	177	177	177	177	177	177	177
λ (Å)	0.71073	0.71073	0.71073	0.71073	0.71073	0.71073	0.71073
a (Å)	9.1981(7)	9.4852(8)	9.5545(10)	46.165(3)	13.0430(11)	19.215(3)	11.7012(10)
b (Å)	9.9374(7)	11.6854(10)	9.8481(10)	12.2340(8)	13.1103(11)	12.2280(19)	12.4231(11)
c (Å)	17.5546(13)	32.866(3)	17.4990(18)	34.353(2)	13.5126(11)	20.500(3)	13.0885(12)
α (°)	79.070(1)	90	78.387(2)	90	71.899(1)	90	73.695(2)
β (°)	80.225(1)	90	81.246(2)	90	67.271(1)	107.805(2)	71.296(2)
γ (°)	79.997(1)	90	82.425(2)	90	82.508(1)	90	63.149(2)
V (Å ³)	1535.9(2)	3642.8(5)	1585.3(3)	19402(2)	2025.6(3)	4586.0(12)	1586.9(2)
Space Group	P-1	P2(1)2(1)2(1)	P-1	Cmca	P-1	P2(1)/c	P-1
Z	2	4	2	28	1	4	2
D ^{calcd} (g/cm ³)	1.483	1.187	1.206	1.371	1.466	1.423	1.278
μ (cm ⁻¹)	5.427	6.390	7.91	16.48	6.110	5.780	7.99
R1, wR2 (I>2σ(I))	0.0274, 0.0612	0.0492, 0.0844	0.0464, 0.0934	0.0602, 0.1217	0.0302, 0.0671	0.0516, 0.0909	0.0488, 0.1225

$$R1 = \frac{\sum ||F_o| - |F_c||}{\sum |F_o|}, wR2 = \left\{ \frac{\sum [w(F_o^2 - F_c^2)^2]}{\sum [w(F_o^2)]} \right\}^{1/2}$$

2.4.5. Syntheses of Compounds.

[PhBP^{*i*Pr}₃]TI (2.1). Preparation of ^{*i*}Pr₂PMe. ^{*i*}Pr₂PCl (24 g, 0.157 mol) was diluted with diethyl ether (250 mL) in a 500 mL Schlenk flask. The ether solution was cooled to -78 °C in a dry ice/acetone bath. To this solution, MeLi (112.3 mL, 0.157 mol) was added via syringe over a period of 40 min. White precipitate formed immediately. The reaction was stirred for 14 h and allowed to warm to room temperature over this time period. The precipitate was filtered on a sintered-glass frit. The volatiles from the supernatant were removed in vacuo, which resulted in further precipitation of LiCl salts. The resulting liquid was diluted in petroleum ether and filtered through Celite on a sintered-glass frit to remove salt. This process was repeated three times, and the volatiles were then removed in vacuo to afford spectroscopically pure ^{*i*}Pr₂PMe (20.13 g, 97%).

Lithiation of MeP^{*i*Pr}₂.^{7c} Solid ^{*i*}BuLi (7.28 g, 0.113 mol) was added to neat quantity of ^{*i*}Pr₂PMe (15.0 g, 0.113 mol) to form a homogeneous solution in a 50 mL round-bottom Schlenk flask. The reaction was heated to 60 °C for 10 h under a slow purge of nitrogen through a bubbler. The white solid was washed with petroleum ether (1 × 25 mL) and collected on a sintered glass frit (15.05 g, 96%; purity ascertained by ³¹P{¹H} NMR in THF: δ 22.4 ppm).

Preparation of [PhBP^{*i*Pr}₃]TI (2.1). In a 250 mL Schlenk flask, solid ^{*i*}Pr₂PCH₂Li (6.5 g, 0.047 mol) was suspended in diethyl ether to which 1 equiv of TMEDA was added in one portion (5.47 g, 0.047 mol). The flask was sealed with a septum and cooled to -78 °C in a dry ice/acetone bath. A toluene solution (15 mL) of PhBCl₂ (2.49 g, 0.016 mol) was added dropwise to the ether solution over a period of 5 min. Salt precipitation was evident within a few minutes after the borane was added. The solution was allowed

to warm to room temperature over a period of 10 h, at which time the solution was filtered through Celite on a sintered glass frit to remove the precipitate. Formation of the product was evident by ^{31}P NMR, which showed a single broad resonance at 4 ppm. Solid TIPF_6 (5.48 g, 0.016 mol) was dissolved in THF and added to the ether solution. Some formation of thallium metal was evident along with the precipitation of salts upon the addition of the TIPF_6 solution. The precipitate was collected on a glass frit. Petroleum ether (25 mL) was added to the supernatant, and the solution was cooled to $-33\text{ }^\circ\text{C}$ overnight, which resulted in the precipitation of a white crystalline solid. The supernatant was decanted, and the solids were washed with acetonitrile (35 mL). The remaining solids were dissolved in a mixture of toluene (3 mL) and petroleum ether (3 mL). The solution was recrystallized by cooling to $-33\text{ }^\circ\text{C}$ overnight, affording analytically pure material (6.2 g, 58%). ^1H NMR (C_6D_6 , 300 MHz): δ 7.97 (m, 2H, H_o BPh), 7.59 (t, 2H, H_m BPh), 7.31 (t, 1H, H_p BPh), 1.89 (septet, 6H, $\text{P}(\text{CH}(\text{CH}_3)_2)$), 1.20 (m, 6H, $\text{B}(\text{CH}_2\text{P}^i\text{Pr}_2)$), 1.05 (dd, 36H, $\text{P}(\text{CH}(\text{CH}_3)_2)$). $^{13}\text{C}\{^1\text{H}\}$ NMR (C_6D_6 , 75.409 MHz): δ 158 (m, C_{ipso} BPh), 132 (s, C_o BPh), 128 (s, C_m BPh), 124 (s, C_p BPh), 24.2 (dd, $\text{P}(\text{CH}(\text{CH}_3)_2)$), 20.6 (s, $\text{P}(\text{CH}(\text{CH}_3)_2)$), 15 (m, $\text{B}(\text{CH}_2\text{P}^i\text{Pr}_2)$). $^{31}\text{P}\{^1\text{H}\}$ NMR (C_6D_6 , 121.4 MHz): δ 24.3 (dd, $^1J_{203\text{Tl-P}} = 5865\text{ Hz}$, $^1J_{205\text{Tl-P}} = 5913\text{ Hz}$). $^{11}\text{B}\{^1\text{H}\}$ NMR (C_6D_6 , 128.3 MHz): δ -13. Anal. Calcd for $\text{C}_{27}\text{H}_{53}\text{BP}_3\text{Tl}$: C, 47.28; H, 7.79. Found: C, 47.23; H, 7.68.

[PhBP i Pr $_3$]FeCl (2.2). A solution of **2.1** (30.3 mg, 0.044 mmol) in THF (1 mL) was added to a stirring suspension of FeCl_2 (5.6 mg, 0.044 mmol) in THF (2 mL) at room temperature. After stirring for 2 h, the resulting canary-yellow solution was filtered through a Celite pad and then evaporated to dryness in vacuo. The yellow solids were dissolved in benzene (2 mL) and filtered again through a Celite pad. Slow evaporation of

the benzene solution afforded analytically pure, crystalline product (21.9 mg, 87%). Suitable crystals were selected for an X-ray diffraction study. $^1\text{H NMR}$ (C_6D_6 , 300 MHz): δ 42.5 (s), 20.0 (s), 18.5 (s), 4.16 (bs), 2.03 (bs), -17.6 (bs), -36.3 (bs). UV-vis (C_6H_6) λ_{max} , nm (ϵ): 422 (550). Evans Method (C_6D_6): 5.23 μB . Anal. Calcd for $\text{C}_{27}\text{H}_{53}\text{BClFeP}_3$: C, 56.62; H, 9.33. Found: C, 56.22; H, 9.32.

[PhBP^{iPr}₃]CoCl (2.3). A solution of **2.1** (51.3 mg, 0.075 mmol) in THF (1 mL) was added to a stirring suspension of CoCl_2 (9.7 mg, 0.075 mmol) in THF (2 mL) at room temperature. After stirring for 2 h, the resulting aqua-green solution was filtered through a Celite pad and then evaporated to dryness in vacuo. The aqua-green solids were dissolved in benzene (2 mL) and filtered again through a Celite pad. Slow evaporation of the benzene solution afforded analytically pure, crystalline product (38.3 mg, 89%). Suitable crystals were selected for an X-ray diffraction study. $^1\text{H NMR}$ (C_6D_6 , 300 MHz): δ 40.5 (bs), 24.7 (bs), 11.7 (s), 8.68 (s), 6.91 (s), 3.64 (bs). UV-vis (C_6H_6) λ_{max} , nm (ϵ): 610 (1140), 720 (1350). Evans Method (C_6D_6): 4.12 μB . Anal. Calcd for $\text{C}_{27}\text{H}_{53}\text{BClCoP}_3$: C, 56.32; H, 9.28. Found: C, 56.29; H, 9.45.

[PhBP^{iPr}₃]CoI (2.4). A solution of **2.1** (50.0 mg, 0.073 mmol) in THF (1 mL) was added to a stirring suspension of CoI_2 (22.0 mg, 0.073 mmol) in THF (2 mL) at room temperature. After stirring for 2 h, the resulting green solution was filtered through a Celite pad and then evaporated to dryness in vacuo. The green solids were dissolved in benzene (2 mL) and filtered again through a Celite pad. Slow evaporation of the benzene solution afforded analytically pure crystalline product (44.7 mg, 92%). Suitable crystals were selected for an X-ray diffraction study. $^1\text{H NMR}$ (C_6D_6 , 300 MHz): δ 41.6 (bs), 24.1 (bs), 12.8 (s), 9.03 (s), 7.23 (s), 5.86 (s), 3.24 (bs). UV-vis (C_6H_6) λ_{max} , nm (ϵ): 660 (676),

745 (1630). Evans Method (C₆D₆): 4.10 μ B. Anal. Calcd for C₂₇H₅₃BCoIP₃: C, 48.60; H, 8.01. Found: C, 47.84; H, 7.91.

{[PhBP^{*i*Pr}]₃Ru(μ -Cl)]₂ (2.5). A solution of **2.1** (80 mg, 0.12 mmol) in 2 mL of THF was added to a stirring solution of RuCl₂(PPh₃)₃ (140 mg, 0.12 mmol) in THF (5 mL) at room temperature. After stirring for 4 h, the brown solution was filtered through a sintered-glass frit to remove insolubles. The volatiles were removed in vacuo to yield a brown solid. The solid was dissolved in CH₂Cl₂ and filtered through a Celite plug to remove TiCl₄. A red-brown solid was precipitated by vapor diffusion of petroleum ether into CH₂Cl₂, affording analytically pure material (112 mg, 78%). ¹H NMR (C₆D₆, 300 MHz): δ 7.81 (m, 2H), 7.45 (t, *J* = 7.6 Hz, 2H), 7.28 (m, 1H), 2.68 (bs, 6H), 1.65 (m, 18H), 1.18 (m, 6H). ³¹P{¹H} NMR (C₆D₆, 121.4 MHz): δ 47.5. ¹³C{¹H} NMR (C₆D₆, 75.409 MHz): δ 157, 132, 127, 124, 25 (m), 20, 15 (m). ¹¹B{¹H} NMR (C₆D₆, 128.3 MHz): δ -7.2. Anal. Calcd for C₅₄H₁₀₆B₂Cl₂P₆Ru₂: C, 52.48; H, 8.64. Found: C, 52.38; H, 8.66.

{[PhBP₃]Ru(μ -Cl)]₂ (2.6). A solution of [BP₃][Ti]^{1b} (40 mg, 0.045 mmol) in 2 mL of THF was added to a stirring solution of RuCl₂(PPh₃)₃ (55 mg, 0.045 mmol) in THF (2 mL) at room temperature. After stirring for 4 h, the solution was filtered through a Celite plug to remove insolubles. Vapor diffusion of petroleum ether into the crude THF solution precipitated brown crystals, affording analytically pure material (38 mg, 97%). A suitable crystal was selected for X-ray analysis. ¹H NMR (CDCl₃, 300 MHz, 25 °C): δ 7.86 (d, *J* = 6.6 Hz, 2 H), 7.54 (t, *J* = 8.4 Hz, 11H), 7.42 (t, *J* = 7.5 Hz, 2H), 7.31 (t, *J* = 7.5 Hz, 2H), 7.02 (m, 18H), 1.63 (m, 6H). ³¹P{¹H} NMR (CDCl₃, 121.4 MHz, 25 °C):

δ 64 (s). $^{11}\text{B}\{^1\text{H}\}$ NMR (CDCl_3 , 128.3 MHz): δ 10.7 (s). Anal. Calcd for $\text{C}_{90}\text{H}_{82}\text{B}_2\text{Cl}_2\text{P}_6\text{Ru}_2$: C, 65.75; H, 5.03. Found: C, 65.72; H, 5.12.

[PhBP^{*i*Pr}₃]FeCl(CO) (2.7). A solution of **2.2** (20 mg, 0.035 mmol) in benzene (1 mL) was sparged with CO gas for 1 min while stirring vigorously at room temperature. The color changed from canary-yellow to a gold hue immediately upon introduction of the CO gas. After stirring for 0.5 h, the resulting golden solution was evaporated to dryness in vacuo to afford analytically pure material (20.2 mg, 98%). ^1H NMR (C_6D_6 , 300 MHz): δ 7.83 (m, 2H), 7.55 (t, $J = 7.8$ Hz, 2H), 7.31 (m, 1H), 2.71 (bs, 1H), 2.08 (bs, 1H), 1.75 (m, 1H), 1.55 (dq, $J = 6.6, 35$ Hz, 5H), 1.18 (m, 8H), 0.87 (dd, $J = 7.2, 12$ Hz, 3H), 0.60 (m, 2H), 0.29 (s, 1H). $^{31}\text{P}\{^1\text{H}\}$ NMR (C_6D_6 , 121.4 MHz): δ 67.5 (t, $J = 50.3$ Hz, 1P), 41.9 (d, $J = 50$ Hz, 2P). $^{11}\text{B}\{^1\text{H}\}$ NMR (C_6D_6 , 128.3 MHz): δ -7.2. IR: ($\text{C}_6\text{H}_6/\text{KBr}$) $\nu_{\text{CO}} = 2020$ cm^{-1} . Anal. Calcd for $\text{C}_{28}\text{H}_{53}\text{BClFeOP}_3$: C, 55.98; H, 8.89. Found: C, 56.02; H, 8.78.

[PhBP^{*i*Pr}₃]CoCl(CO) (2.8). A solution of **2.3** (19.5 mg, 0.034 mmol) in benzene (1 mL) was sparged with CO gas for 1 min while stirring vigorously at room temperature. The color changes from aqua-green to an intense green immediately upon introduction of the CO gas. After stirring for 0.5 h, the resulting green solution was evaporated to dryness in vacuo to afford analytically pure material (20.3 mg, 99%). ^1H NMR (C_6D_6 , 300 MHz): δ 24.8 (bs), 12.1 (s), 8.68 (s), 6.91 (s), 3.64 (bs), -0.86 (s). Evans Method (C_6D_6): 2.24 μ_{B} . IR: ($\text{C}_6\text{H}_6/\text{KBr}$) $\nu_{\text{CO}} = 2010$ cm^{-1} . Anal. Calcd for $\text{C}_{28}\text{H}_{53}\text{BClCoOP}_3$: C, 55.69; H, 8.85. Found: C, 55.66; H, 8.89.

[PhBP^{*i*Pr}₃]Co(CO)₂ (2.9). A solution of **2.4** (9.1 mg, 0.014 mmol) in benzene (1 mL) was sparged with CO gas for 1 min while stirring vigorously at room temperature.

The color changes from green to an intense lime-green immediately upon introduction of the CO gas. After stirring for 0.5 h, the resulting green solution was evaporated to dryness in vacuo. The lime-green solids were dissolved in a mixture of benzene (1 mL) and petroleum ether (1 mL) and filtered through a Celite pad. The volatiles were then removed in vacuo to afford analytically pure material (7.4 mg, 92%). ^1H NMR (C_6D_6 , 300 MHz): δ 7.92 (m, 2H), 7.80 (m, 2H), 7.44 (m, 1H), 2.55 (m, 6H), 1.86 (m, $J = 7.2$ Hz, 18H), 0.86 (m, 6H). $^{13}\text{C}\{^1\text{H}\}$ NMR (C_6D_6 , 75.409 MHz): δ 182, 156, 130, 127, 123, 24.4 (m), 19, 16 (m). $^{31}\text{P}\{^1\text{H}\}$ NMR (CDCl_3 , 121.4 MHz, 25 °C): δ 56. IR: ($\text{C}_6\text{H}_6/\text{KBr}$) $\nu_{\text{CO}} = 1990, 1904\text{ cm}^{-1}$. Anal. Calcd for $\text{C}_{29}\text{H}_{53}\text{BCoO}_2\text{P}_3$: C, 58.40; H, 8.96. Found: C, 58.21; H, 8.99.

$[\text{PhBP}^{\text{iPr}}_3]\text{RuCl}(\text{CO})_2$ (2.10). To a solution of **2.5** (40 mg, 0.032 mmol) in 5 mL THF was added 1 atm of CO gas (through a septum in a 20 mL vial) at room temperature. The vial was stirred at room temperature until the solution color changed from red-brown to a pale yellow, at which point the excess CO gas was removed via an Ar purge. The solution was filtered through a Celite plug in air to remove insolubles. The solution was then evaporated to dryness in vacuo to afford analytically pure material (40 mg, 92%). ^1H NMR (C_6D_6 , 300 MHz): δ 7.80 (m, 2H), 7.60 (t, $J = 7.2$ Hz, 2H), 7.30 (m, 1H), 3.01 (bs, 1H), 2.28 (bs, 1H), 1.78 (m, 1H), 1.65 (dq, $J = 6.6, 35$ Hz, 6H), 1.18 (m, 8H), 0.90 (dd, $J = 7.2, 12$ Hz, 3H), 0.60 (m, 2H). $^{31}\text{P}\{^1\text{H}\}$ NMR (C_6D_6 , 121.4 MHz): δ 56 (t, $J = 46$ Hz, 1P), 35 (d, $J = 48$ Hz, 2P). $^{11}\text{B}\{^1\text{H}\}$ NMR (C_6D_6 , 128.3 MHz): δ -9.2. IR: ($\text{CH}_2\text{Cl}_2/\text{KBr}$) $\nu_{\text{CO}} = 2045, 1993\text{ cm}^{-1}$. Anal. Calcd for $\text{C}_{29}\text{H}_{53}\text{BClO}_2\text{P}_3\text{Ru}$: C, 51.68; H, 7.93. Found: C, 51.25; H, 7.91.

[PhBP₃]RuCl(CO)₂ (2.11). To a solution of **2.6** (40 mg, 0.024 mmol) in 5 mL of THF was added 1 atm of CO gas (through a septum in a 20 mL vial) at room temperature. The vial was stirred until the solution color changed from yellow-brown to colorless, at which point the excess CO gas was removed via an Ar purge. The solution was filtered through a Celite plug in air to remove insolubles. The solution was then evaporated to dryness in vacuo to afford analytically pure material (41 mg, 96%). ¹H NMR (CDCl₃, 300 MHz): δ 7.86 (d, *J* = 6.6 Hz, 2 H), 7.47 (m, 16H), 7.00 (m, 18H), 1.98 (m, 4H), 1.82 (bs, 2H). ³¹P{¹H} NMR (CDCl₃, 121.4 MHz, 25 °C): δ 39.9 (t, *J* = 32 Hz), 11.3 (d, *J* = 32 Hz). IR: (CH₂Cl₂/KBr) ν_{CO} = 2068, 2021 cm⁻¹. Anal. Calcd for C₄₇H₄₁BClO₂P₃Ru: C, 64.29; H, 4.71. Found: C, 64.25; H, 4.58.

[PhBPⁱPr₃]RuCl(PMe₃) (2.12). To a solution of **2.5** (40 mg, 0.032 mmol) in 5 mL of toluene was added an excess of PMe₃ (10 mg, 0.13 mmol). After stirring for 4 h at 50 °C, the volatiles were removed in vacuo to afford a brick-red oil. Red-brown solids were precipitated by cooling the toluene solution at -33 °C overnight, affording analytically pure material (40.8 mg, 91%). ¹H NMR (C₆D₆, 300 MHz): δ 7.74 (m, 2H), 7.45 (t, *J* = 7.6 Hz, 2H), 7.28 (m, 1H), 2.68 (bs, 6H), 1.65 (m, 18H), 1.18 (m, 6H), 0.72 (b, 9H). ³¹P{¹H} NMR (C₆D₆, 121.4 MHz): δ 44 (very broad), -4.4 (q, *J* = 77 Hz). ¹³C{¹H} NMR (C₆D₆, 75.409 MHz): δ 157, 132, 127, 124, 24 (m), 20, 18 (m), 15 (m). Anal. Calcd for C₃₀H₆₂BClP₄Ru: C, 51.92; H, 9.00. Found: C, 50.96; H, 8.99.

[PhBP₃]RuCl(PMe₃) (2.13). To a solution of **2.6** (40 mg, 0.024 mmol) in 5 mL toluene was added an excess of PMe₃ (10 mg, 0.13 mmol). After stirring for 4 h at 50 °C, the volatiles were removed in vacuo to afford a brick-red solid. Crystals were afforded by vapor diffusion of petroleum ether into THF, providing analytically pure material (38.4

mg, 88%). A crystal was selected for an X-ray diffraction study. ^1H NMR (CDCl_3 , 300 MHz): δ 7.84 (d, $J = 6.6$ Hz, 2 H), 7.53 (t, $J = 8.4$ Hz, 11H), 7.47 (t, $J = 7.5$ Hz, 2H), 7.23 (t, $J = 7.5$ Hz, 2H), 6.95-7.07 (m, 18H), 1.63 (m, 6H), 0.67 (bs, 9H). $^{31}\text{P}\{^1\text{H}\}$ NMR (CDCl_3 , 121.4 MHz): δ 54 (bm), 2.50 (q, $J = 74.8$ Hz). $^{11}\text{B}\{^1\text{H}\}$ NMR (CDCl_3 , 128.3 MHz): δ 10.8 (s). Anal. Calcd for $\text{C}_{48}\text{H}_{50}\text{BClP}_4\text{Ru}$: C, 64.19; H, 5.61. Found: C, 64.22; H, 5.60.

[PhB(CH₂P(O)^{*i*}Pr₂)₂(CH₂P^{*i*}Pr₂)]CoCl (2.14). Dioxygen (1 mL, 0.045 mmol) was added via syringe to a solution of **2.3** (25.7 mg, 0.045 mmol) in benzene (1 mL), and then, the mixture was stirred vigorously at room temperature. The color changes from aqua-green to an intense blue. After stirring for 2 h, the resulting blue solution was evaporated to dryness. Crystals were afforded by slow evaporation of a benzene solution affording analytically pure material (24.0 mg, 87%). ^1H NMR (C_6D_6 , 300 MHz): δ 24.5, 11.7, 8.72, 6.92, 3.6 (b), 0.88, -0.66. Evans Method (C_6D_6): 4.23 μB . Anal. Calcd for $\text{C}_{27}\text{H}_{53}\text{BClCoO}_2\text{P}_3$: C, 53.35; H, 8.79. Found: C, 52.69; H, 8.86.

[PhB(CH₂P(O)^{*i*}Pr₂)₃]CoCl (2.15). Dioxygen (3 mL, 0.135 mmol) was added via syringe to a solution of **2.3** (25.7 mg, 0.045 mmol) in benzene (1 mL) and then stirred vigorously at room temperature. The color changes from aqua-green to an intense blue. After stirring for 6 h, the resulting blue solution was evaporated to dryness to afford analytically pure material (24.2 mg, 86%). ^1H NMR (C_6D_6 , 300 MHz): δ 24.8, 12.1, 8.25, 6.86, 3.55 (b), 0.68, -0.99. Evans Method (C_6D_6): 4.24 μB . Anal. Calcd for $\text{C}_{27}\text{H}_{53}\text{BClCoO}_3\text{P}_3$: C, 51.98; H, 8.56. Found: C, 51.33; H, 8.54.

Crystals of **2.14** and **2.15** were grown by letting a concentrated solution of **2.3** to stand for 12 h at room temperature under an atmosphere of air. While the majority of the

species formed was **2.14** (81%), a small fraction (19%) of the tris(phosphineoxide) **2.15** was also formed and cocrystallized.

References Cited

1. (a) Jenkins, D. M.; Di Bilio, A. J.; Allen, M. J.; Betley, T. A.; Peters, J. C. *J. Am. Chem. Soc.* **2002**, *124*, 15336. (b) Shapiro, I. R.; Jenkins, D. M.; Thomas, J. C.; Day, M. W.; Peters, J. C. *Chem. Commun.* **2001**, 2152.
2. (a) Jenkins, D. M.; Betley, T. A.; Peters, J. C. *J. Am. Chem. Soc.* **2002**, *124*, 11238. (b) Brown, S. D.; Betley, T. A.; Peters, J. C. *J. Am. Chem. Soc.* **2003**, *125*, 322.
3. (a) For some relevant references see: Schebler, P. J.; Mandimutsira, B. S.; Riordan, C. G.; Liable-Sands, L. M.; Incarvito, C. D.; Rheingold, A. L. *J. Am. Chem. Soc.* **2001**, *123*, 331. (b) Gorrell, I. B.; Parkin, G. *Inorg. Chem.* **1990**, *29*, 2452. (c) Bunker, T. J.; Hascall, T.; Cowley, A. R.; Rees, L. H.; O'Hare, D. *Inorg. Chem.* **2001**, *40*, 3170. (d) Kitajima, N.; Fujisawa, K.; Moro-oka, Y. *J. Am. Chem. Soc.* **1990**, *112*, 3210. (e) Churchill, M. R.; DeBoer, B. G.; Rotella, F. J.; Salah, O. M. A.; Bruce, M. I. *Inorg. Chem.* **1975**, *14*, 2051. (f) Belderrain, T. R.; Parreque, M.; Carmona, E.; Gutierrez-Puebla, E.; Monge, M. A.; Ruiz-Valero, C. *Inorg. Chem.* **2002**, *41*, 425. (g) Carrier, S. M.; Ruggiero, C. E.; Tolman, W. B.; Jameson, G. B. *J. Am. Chem. Soc.* **1992**, *114*, 4407.
4. Detrich, J. L.; Konecny, R.; Vetter, W. M.; Doren, D.; Rheingold, A. L.; Theopold, K. H. *J. Am. Chem. Soc.* **1996**, *118*, 1703.
5. Kisko, J. L.; Hascall, T.; Parkin, G. *J. Am. Chem. Soc.* **1998**, *120*, 1056.
6. (a) Peters, J. C.; Feldman, J. D.; Tilley, T. D. *J. Am. Chem. Soc.* **1999**, *121*, 9871. (b) Barney, A. A.; Heyduk, A. F.; Nocera, D. G. *Chem. Commun.* **1999**, 23, 2379.
7. (a) Thomas, J. C.; Peters, J. C. *J. Am. Chem. Soc.* **2001**, *123*, 5100. (b) Betley, T. A.; Peters, J. C. *Inorg. Chem.* **2002**, *41*, 6541. (c) Thomas, J. C.; Peters, J. C. *Inorg. Chem.* **2003**, *42*, 5055.

-
8. (a) Ge, P.; Haggerty, B. S.; Rheingold, A. L.; Riordan, C. G. *J. Am. Chem. Soc.* **1994**, *116*, 8406. (b) Schebler, P. J.; Riordan, C. G.; Guzei, I. A.; Rheingold, A. L. *Inorg. Chem.* **1998**, *37*, 4754.
9. Karsch, H. H.; Schmidbaur, H. *Z. Naturforsch.* **1977**, *32b*, 762.
10. (a) Rhodes, L. F.; Sorato, C.; Venanzi, L. M.; Bachechi, F. *Inorg. Chem.* **1988**, *27*, 604. (b) Rhodes, L. F.; Venanzi, L. M.; Sorato, C.; Albinati, A. *Inorg. Chem.* **1986**, *25*, 3335.
11. Another case of an isolated, coordinatively unsaturated ruthenium species featuring a sterically encumbered hydrotris(3,5-diisopropylpyrazolyl)borato ligand features an agostic C-H bond interaction occupying the sixth coordination site on Ru: (a) Takahashi, Y.; Hikichi, S.; Akita, M.; Moro-Oka, Y. *Organometallics* **1999**, *18*, 2571. Related transiently stable species that feature agostic interactions have been studied: (b) Trimmel, G.; Slugovc, C.; Wiede, P.; Mereiter, K.; Sapunov, V. N.; Schmid, R.; Kirchner, K. *Inorg. Chem.* **1997**, *36*, 1076. (c) Tenorio, M. A. J.; Tenorio, M. J.; Puerta, M. C.; Valerga, P. *J. Chem. Soc., Dalton Trans.* **1998**, 3601.
12. See ref 1a and references therein.
13. Sealy, R.; Hyde, J. S.; Antholine, W. E. *Modern Physical Methods in Biochemistry*; Neuberger, A., Van Deenen, L. L. M., Eds.; Elsevier: New York, 1985; p 69.
14. Stelzer, O.; Sheldrick, W. S.; Subramanian, J. *J. Chem. Soc., Dalton Trans.* **1976**, 966.
15. (a) Pilbrow, J. R. *Transition Ion Electron Paramagnetic Resonance*; Clarendon Press: Oxford, 1990. (b) Aasa, R.; Vanngard, T. *J. Magn. Reson.* **1975**, *19*, 308.
16. Preparation and spectroscopic information included in the Supporting Information.

-
17. A series of thoroughly characterized, 5-coordinate [PhBP₃]Co(II) complexes, including [PhBP₃]CoBr(CO), has been prepared and will be reported in due course. Synthetic and characterization data for [PhBP₃]CoBr(CO) were reported in the Supporting Information of ref 1a.
18. Oxygenation of related (triphos)Co²⁺ complexes did not produce similarly isolable species. See: Hienze, K.; Huttner, G.; Zsolnai, L. *Chem. Ber.* **1997**, *130*, 1393.
19. Detrich, J. L.; Reinaud, O. M.; Rheingold, A. L.; Theopold, K. H. *J. Am. Chem. Soc.* **1995**, *117*, 11745.
20. King, R. B.; Bisnette, M. B. *J. Organomet. Chem.* **1967**, *8*, 287.
21. King, R. B.; Bisnette, M. B. *J. Organomet. Chem.* **1973**, *56*, 345.
22. Dapporto, P.; Midollini, S.; Sacconi, L. *Inorg. Chem.* **1975**, *14*, 1643.
23. Siegl, W. O.; Lapporte, S. J.; Collman, J. P. *Inorg. Chem.* **1973**, *12*, 674.
24. For example, see refs 7b,c. Also see: (a) Thomas, J. C.; Peters, J. C. *J. Am. Chem. Soc.* **2003**, *125*, 8870. (b) Betley, T. A.; Peters, J. C. *Angew. Chem., Int. Ed.* **2003**, *42*, 2385.
25. Fagan, P. J.; Mahoney, W. S.; Calabrese, J. C.; Williams, I. D. *Organometallics* **1990**, *9*, 1843.
26. Brown, D. A.; Lyons, H. J.; Sane, R. T. *Inorg. Chim. Acta.* **1970**, *4*, 621.
27. Tenorio, M. A. J.; Tenorio, M. J.; Puerta, M. C.; Valerga, P. *J. Chem. Soc., Dalton Trans.* **1998**, 3601.
28. Hallman, P. S.; Stephenson, T. A.; Wilkinson, G. *Inorg. Synth.* **1970**, *12*, 237.
29. Kahn, O. *Molecular Magnetism*; VCH Publishers: New York, 1993; pp 1-10.